

# Methylation of Mercury by Bacteria Exposed to Dissolved, Nanoparticulate, and Microparticulate Mercuric Sulfides

Tong Zhang,<sup>†</sup> Bojeong Kim,<sup>‡</sup> Clément Levard,<sup>§</sup> Brian C. Reinsch,<sup>||</sup> Gregory V. Lowry,<sup>||</sup> Marc A. Deshusses,<sup>†</sup> and Heileen Hsu-Kim<sup>†,\*</sup>

<sup>†</sup>Department of Civil & Environmental Engineering, Duke University, 121 Hudson Hall, Box 90287, Durham, North Carolina 27708, United States

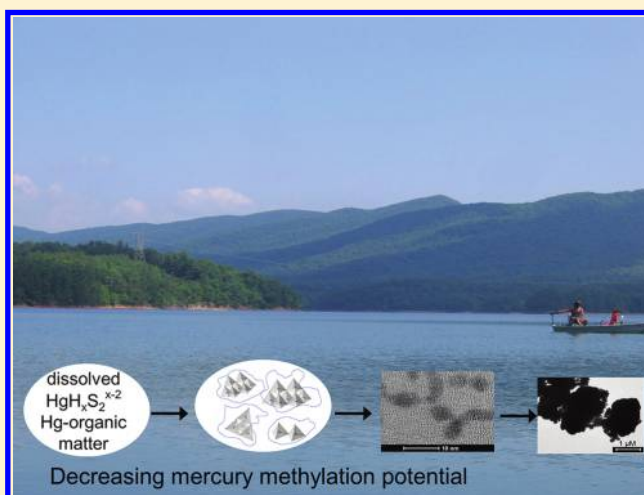
<sup>‡</sup>Department of Geosciences, Virginia Polytechnic Institute and State University, Blacksburg, Virginia 24061, United States

<sup>§</sup>Department of Geological & Environmental Sciences, Stanford University, Stanford, California 94305, United States

<sup>||</sup>Department of Civil & Environmental Engineering, Carnegie Mellon University, Pittsburgh, Pennsylvania 15213, United States

**S** Supporting Information

**ABSTRACT:** The production of the neurotoxic methylmercury in the environment is partly controlled by the bioavailability of inorganic divalent mercury (Hg(II)) to anaerobic bacteria that methylate Hg(II). In sediment porewater, Hg(II) associates with sulfides and natural organic matter to form chemical species that include organic-coated mercury sulfide nanoparticles as reaction intermediates of heterogeneous mineral precipitation. Here, we exposed two strains of sulfate-reducing bacteria to three forms of inorganic mercury: dissolved Hg and sulfide, nanoparticulate HgS, and microparticulate HgS. The bacteria cultures exposed to HgS nanoparticles methylated mercury at a rate slower than cultures exposed to dissolved forms of mercury. However, net methylmercury production in cultures exposed to nanoparticles was 6 times greater than in cultures treated with microscale particles, even when normalized to specific surface area. Furthermore, the methylation potential of HgS nanoparticles decreased with storage time of the nanoparticles in their original stock solution. In bacteria cultures amended with nano-HgS from a 16 h-old nanoparticle stock, 6–10% of total mercury was converted to methylmercury after one day. In contrast, 2–4% was methylated in cultures amended with nano-HgS that was aged for 3 days or 1 week. The methylation of mercury derived from nanoparticles (in contrast to the larger particles) would not be predicted by equilibrium speciation of mercury in the aqueous phase (<0.2  $\mu\text{m}$ ) and was possibly caused by the disordered structure of nanoparticles that facilitated release of chemically labile mercury species immediately adjacent to cell surfaces. Our results add new dimensions to the mechanistic understanding of mercury methylation potential by demonstrating that bioavailability is related to the geochemical intermediates of rate-limited mercury sulfide precipitation reactions. These findings could help explain observations that the “aging” of mercury in sediments reduces its methylation potential and provide a basis for assessing and remediating methylmercury hotspots in the environment.



## INTRODUCTION

Methylmercury (MeHg) production in the aquatic environment is primarily mediated by anaerobic bacteria, particularly sulfate reducing bacteria (SRB).<sup>1,2</sup> Microbial mercury methylation has been extensively studied for decades.<sup>3</sup> Nevertheless, our knowledge of the mechanisms of this process is rather limited. The speciation (and subsequent bioavailability to methylating bacteria<sup>4</sup>) of inorganic divalent mercury (Hg(II)) is controlled by inorganic sulfide S(-II) and dissolved natural organic matter (NOM) that can strongly bind Hg<sup>2+</sup>.<sup>5–7</sup>

In the past, mercury bioavailability and methylation potential has been predicted based on chemical equilibrium models of

dissolved mercury complexes in porewater (nominally defined by the fraction passing through 0.2 or 0.45  $\mu\text{m}$  filters).<sup>6</sup> This approach presumes that mercury uptake is controlled by hydrophobic partitioning of dissolved neutrally charged Hg-sulfide species that passively diffuse through the cell membranes of methylating bacteria. Thus, the methylation

**Special Issue:** Transformations of Nanoparticles in the Environment

**Received:** September 10, 2011

**Revised:** December 4, 2011

**Accepted:** December 6, 2011

**Published:** December 6, 2011

potential from this approach is estimated from the concentrations of neutrally charged Hg sulfide species calculated at chemical equilibrium. Our previous research has shown that this model is flawed because it must invoke an unknown species,  $\text{HgS}^0_{(\text{aq})}$  that may represent nanoparticulate HgS rather than a mononuclear aqueous complex.<sup>8</sup> Here, we hypothesize that mercury speciation in anaerobic settings represent a mixture of dissolved, nanoparticulate, and bulk scale forms of HgS whose concentrations and bioavailability cannot be represented by conventional equilibrium models.

Mercuric sulfide (HgS) nanoparticles are known to exist in nature<sup>9–11</sup> and can account for a portion of mercury passing through 0.2 or 0.45  $\mu\text{m}$  filters,<sup>12–14</sup> an operational cutoff often used to separate “dissolved” from particulate. In filtered porewater, mercury is often supersaturated with respect to  $\text{HgS}_{(\text{s})}$ .<sup>8</sup> As with other minerals, the precipitation of  $\text{HgS}_{(\text{s})}$  involves nanoparticles that can be prevented from growing or aggregating by NOM.<sup>8,15</sup> Nanoparticles of HgS and other metal sulfides have been observed in anaerobic sediments and other settings where active precipitation was occurring,<sup>9–11,16,17</sup> yet the role of nanoscale HgS for biomethylation has not been elucidated. As a result, accurate prediction of MeHg production and accumulation in the environment remains elusive.

Nanoparticles are not simply smaller versions of larger particles. Indeed, nanoparticles exhibit unique reactivity due to the high surface area-to-mass ratio of nanoscale materials and resulting alterations in lattice structure and surface chemistry.<sup>18</sup> Conventional models of metal bioavailability use a chemical equilibrium speciation approach that presumes all particles (nano or otherwise) to be unavailable to microbes, yet this approach neglects properties such as enhanced solubility and greater deposition of nanoscale materials directly onto cell surfaces.<sup>19–21</sup> Thus, nanoscale-specific reactivity of mercury may be contributing to its bioavailability and methylation potential in the environment.

In this study, we examined the methylation potential of various forms of mercuric sulfides by exposing fermentatively cultured SRB strains, *Desulfobulbus propionicus* 1pr3 and *Desulfovibrio desulfuricans* ND132, to three forms of mercury: dissolved  $\text{Hg}(\text{NO}_3)_2$  freshly mixed with  $\text{Na}_2\text{S}$  (dissolved Hg+S exposure), humic-stabilized HgS nanoparticles, and commercially purchased HgS microparticles. These forms of mercury represented three different aging states of mercury in sulfidic sediments. We also characterized the structure of the HgS nanoparticles and assessed the speciation of mercury in the culture media during the incubation experiments.

## MATERIALS AND METHODS

**Microorganisms and Culture Conditions.** *Desulfobulbus propionicus* 1pr3 (ATCC 33891) and *Desulfovibrio desulfuricans* ND132 (C. Gilmour, Smithsonian Environmental Research Center) were utilized as the test microorganisms. These strains were cultured in Hungate tubes (Bellco Glass) placed in an anaerobic chamber. Cell growth was monitored by optical density ( $\text{OD}_{660}$ ) and protein content.<sup>22</sup> The bacterial cultures were maintained between experiments on sulfate-containing medium. Prior to mercury methylation bioassays, the cultures were transferred three times in fermentative media that contained 20 mM pyruvate (for 1pr3) or 40 mM fumarate (for ND132) as the organic carbon source, 0.15 mM Ti-nitrioltriacetic acid (NTA) as the reductant and 10 mg/L resazurin as the redox indicator, according to previous methods.<sup>5,23</sup>

**HgS Particle Preparation.** The Hg stock solution consisted of  $\text{Hg}(\text{NO}_3)_2$  dissolved in 0.1 N  $\text{HNO}_3$ .  $\text{Na}_2\text{S}$  stocks were prepared by dissolving freshly washed and dried crystals of  $\text{Na}_2\text{S}\cdot 9\text{H}_2\text{O}$  (Fisher Scientific) in  $\text{N}_2$ -purged water and were utilized within 4 h of preparation. HgS nanoparticles were synthesized by dissolving 50  $\mu\text{M}$   $\text{Hg}(\text{NO}_3)_2$  and 50  $\mu\text{M}$   $\text{Na}_2\text{S}$  with 10 mg-C  $\text{L}^{-1}$  Suwannee River humic acid (SRHA, International Humic Substances Society) in a solution of 0.1 M  $\text{NaNO}_3$  and 4 mM sodium 4-(2-hydroxyethyl) piperazine-1-ethanesulfonate (HEPES) (pH 7.5, double-filtered to  $<0.1 \mu\text{m}$ ). Depending on the experiments, the Hg–S–NOM nanoparticle stock solution was allowed to age for 16 h to 1 week at room temperature prior to use in the methylation experiments. A microparticulate HgS stock suspension was prepared by adding a commercial metacinnabar powder ( $\beta$ -HgS, Alfa Aesar) into nanopure-filtered water ( $>18 \text{ M}\Omega\text{-cm}$ ). This suspension was mixed end-over-end prior to taking an aliquot for the experiments.

**HgS Particle Characterization.** The average hydrodynamic diameter of HgS nanoparticles and microparticles were analyzed by light-intensity weighted dynamic light scattering (DLS) (Malvern Zetasizer NS). The diameters of the monomers within the aggregates were analyzed by transmission electron microscopy (TEM). BET surface areas of HgS nanoparticles and microparticles were determined using the BET  $\text{N}_2$  adsorption technique (Beckman Coulter SA3100 Surface Area Analyzer). The geometric surface areas of HgS particles were calculated from the individual particle size obtained from TEM images. The geometric surface area calculations assumed spherical particles with a density of 7.71  $\text{g cm}^{-3}$ .<sup>24</sup>

The crystallographic structure of HgS nanoparticles and microparticles was analyzed by synchrotron X-ray diffraction (XRD) performed at the Stanford Synchrotron Radiation Laboratory (SSRL) BL 11–3. The average crystallite diameter  $D$  of nano-HgS was estimated from the broadening of the X-ray diffraction peaks by the Scherrer formula:<sup>25</sup>

$$D = \frac{K\lambda}{\beta \cos \theta} \quad (1)$$

where  $K$  is the constant of proportionality ( $K = 0.9$ ),  $\lambda$  is the X-ray wavelength ( $\lambda = 0.0977 \text{ nm}$ ),  $\beta$  is the peak full width at half maximum (FWHM) in radians and  $\theta$  is the Bragg angle.

The elemental composition of the HgS particles was analyzed by X-ray photoelectron spectrometry (XPS) using a PHI VersaProbe Scanning XPS Microprobe. Additional details on the preparation of samples for these analyses are provided in the Supporting Information (SI) section.

**Mercury Methylation Bioassay.** The bacterial cultures were pregrown in a fermentative medium and incubated until exponential growth phase (19 h for *D. propionicus* 1pr3 and 67 h for *D. desulfuricans* ND132) prior to dosing with mercury. In the dissolved Hg+S exposure,  $\text{Hg}(\text{NO}_3)_2$  and  $\text{Na}_2\text{S}$  were added into the test cultures separately. While we refer to this exposure as “dissolved Hg+S” because of the initial method of dosing, HgS was supersaturated in these cultures and likely consisted of early stage precipitation products (i.e., HgS clusters and nanoparticles). The cultures were also exposed to humic-associated HgS nanoparticles, representing an intermediate stage of heterogeneous HgS precipitation, and microscale crystalline HgS, representing a mercury-bearing mineral encountered in soil and sediments.<sup>9,26</sup> In the dissolved and micro-HgS treatments, SRHA,  $\text{NaNO}_3$  and HEPES were also

**Table 1. Average Size and Surface Area of Humic-HgS Nanoparticles and HgS Microparticles Utilized in Methylation Bioassays<sup>a</sup>**

HgS particles	hydrodynamic diameter (nm) <sup>b</sup>	monomer diameter (nm) <sup>c</sup>	crystallite diameter (nm) <sup>d</sup>	surface area (m <sup>2</sup> g <sup>-1</sup> )	
				BET <sup>e</sup>	Geometric <sup>f</sup>
nanoparticles (aged for 16 h)	25.8 ± 2.9 (n = 10)	3.2 ± 0.8 (n = 110)	5.7 ± 0.1 (n = 3)	47.9	264 ± 72 (n = 110)
nanoparticles (aged for 3 days)	27.6 ± 3.0 (n = 5, p = 0.27)	3.3 ± 0.9 (n = 110, p = 0.14)	5.0 ± 0.3 (n = 3, p = 0.012)	ND	250 ± 63 (n = 110, p = 0.13)
nanoparticles (aged for 1 week)	28.3 ± 4.9 (n = 4, p = 0.25)	3.6 ± 0.7* (n = 110, p = 10 <sup>-5</sup> )	5.7 ± 0.1 (n = 3, p = 0.89)	ND	224 ± 47* (n = 110, p = 2 × 10 <sup>-6</sup> )
microparticles	1457 ± 435* (n = 7, p = 2 × 10 <sup>-8</sup> )	530 ± 367* (n = 78, p = 10 <sup>-25</sup> )	NA	2.5	2.5 ± 1.8* (n = 78, p = 10 <sup>-68</sup> )

<sup>a</sup>Diameters and geometric surface areas were compared to the 16-h HgS nanoparticles using an unpaired two-tailed *t*-test. Values that are statistically different (*p* < 0.01) from the 16-h nanoparticles are indicated by an asterisk (\*). NA: Not available. ND: Not determined. <sup>b</sup>Quantified by light-intensity weighted dynamic light scattering. <sup>c</sup>Estimated from individual monomers observed in TEM images (SI Figure S4). <sup>d</sup>Estimated from the broadening of the X-ray diffraction peak widths by the Scherrer formula (SI Figure S5c). <sup>e</sup>BET surface area quantified by N<sub>2</sub>-gas adsorption. <sup>f</sup>Geometric surface areas (based on approximation of spherical monomers) were calculated from the size of individual particles in TEM images.

added to the test cultures to account for the chemical carryover from the HgS nanoparticle stock in the nano-HgS treatment. The concentration of spiked mercury sulfides was 6–20 nM in micro-HgS treatment and 1–5 nM in all the other treatments. The cultures were continuously mixed end-over-end and stored in an anaerobic chamber during incubation (1–10 days). All mercury methylation bioassays were incubated in the dark at room temperature (25–27 °C). All the bacterial cultures were buffered with 19.2 mM 3-(*N*-morpholino)propanesulfonic acid (MOPS) at pH 7.0–7.3.

At each time point, triplicate vials were sacrificed and subsampled for measurements of total protein and mercury concentration. After subsampling, the remaining cultures were preserved by adding 0.4% (v/v) concentrated hydrochloric acid (HCl) (trace metal grade) and stored at 4 °C prior to MeHg analysis. Two sets of controls were incubated under the same conditions including (1) abiotic control consisting of uninoculated media amended with Hg(NO<sub>3</sub>)<sub>2</sub> and Na<sub>2</sub>S; (2) killed control consisting of autoclaved (121 °C, 30 min) cultures amended with Hg(NO<sub>3</sub>)<sub>2</sub> and Na<sub>2</sub>S after the autoclave step. MeHg concentrations in all control samples were below the detection limit (≤8 pM MeHg) and significantly lower than MeHg in viable cultures amended with Hg(NO<sub>3</sub>)<sub>2</sub> and Na<sub>2</sub>S.

**Chemical Analysis.** MeHg concentration was quantified by distillation, aqueous phase ethylation, gas chromatographic separation, and atomic fluorescence spectrometry (Tekran 2600).<sup>27</sup> Samples for total mercury analysis were first digested with 2–4% (v/v) BrCl for at least 12 h and analyzed by SnCl<sub>2</sub> reduction, gold amalgamation, and cold vapor atomic fluorescence spectrometry.<sup>28</sup>

**Mercury Fractionation by Filtration.** In mercury methylation bioassays, total mercury in a subset of *D. propionicus* 1pr3 cultures was fractionated using filtration. Separate test cultures were filtered with either 0.22 μm polycarbonate (GE Osmonics Labstore) or 0.02 μm aluminum oxide (Whatman) syringe filters. Total mercury concentration in the filtrates was quantified and represented different mercury species: (1) <0.02 μm fraction considered the nominally “dissolved” mercury and likely consisted of aqueous mononuclear mercury complexes (e.g., Hg(OH)<sub>*x*</sub><sup>2-*x*</sup>, Hg(HS)<sub>*x*</sub><sup>2-*x*</sup>) and possibly polynuclear mercury sulfide clusters; (2) 0.02–0.22 μm fraction which contained colloidal mercury (e.g., Hg-S-NOM nanoparticles); and (3) >0.22 μm fraction which contained cell- and/or large particle-associated mercury. Filtration experiments were also performed with bacteria-free

media amended with the three forms of mercury (dissolved Hg+S, nano-HgS, and micro-HgS). These solutions were stored at room temperature and filtered with 0.02 and 0.22 μm filters at multiple time points up to 1 day.

Centrifugation and ultracentrifugation were also used to separate dissolved and nanoparticulate species. Further details are provided in the SI section.

**TEM Analysis of HgS-Amended Cultures.** After 14-h exposure to HgS, cells from 1pr3 cultures were separated by centrifugation, washed with 10 mM phosphate buffered saline (PBS, pH 7.4), and resuspended in a fixative solution containing 4% (v/v) formaldehyde and 2% glutaraldehyde. After storing for 4 h in the fixative, the cells were washed with high purity deionized water (>18 MΩ-cm). This suspension was deposited on a carbon-coated copper grid (200 mesh) and imaged by FEI Tecnai TEM operating at 80 keV (Figure 2b, d, and f) and a JEOL 2000 FX TEM operating at 200 keV with an energy dispersive X-ray (EDX) spectrometer for the element analysis. (SI Figure S7).

**Mercury Ligand Exchange Reactivity.** A subset of mercury-treated media solution (no bacteria) was analyzed for chemical speciation of mercury using a previously developed competitive ligand exchange-solid phase extraction (CLE-SPE) method.<sup>8,29,30</sup> This technique separates labile mercury species from strongly complexed (i.e., inert) mercury species based on the chemical reactivity of mercury in the presence of a competing ligand: glutathione (GSH) or diethyl dithiocarbamate (DEDIC). GSH and DEDIC are both thiol-containing compounds and form strong hydrophilic complexes (HgH<sub>2</sub>(GSH)<sub>2</sub><sup>2-</sup>) or hydrophobic complexes (Hg(DEDIC)<sub>2</sub><sup>0</sup>) with mercury that can be differentiated from the original Hg-sulfide or Hg-NOM species using C<sub>18</sub>-resin solid phase extraction. In the past, researchers have used CLE-SPE to quantify stability constants (assuming that reactions reach equilibrium). Here, we do not imply equilibrium but simply use this method to quantify the reactivity of the Hg for thiol-ligand exchange.

The bacteria-free media containing mercury (either dissolved Hg+S, nano-HgS, or micro-HgS) were sampled at the beginning and end of a one-day holding period at room temperature. These samples were divided into three aliquots that were amended with either 0.1 mM GSH, 0.1 mM DEDIC, or no additional thiol. After 1 h of reaction time, the samples were filtered through a C<sub>18</sub>-resin packed column. The hydrophobic fraction was defined by mercury retained by the

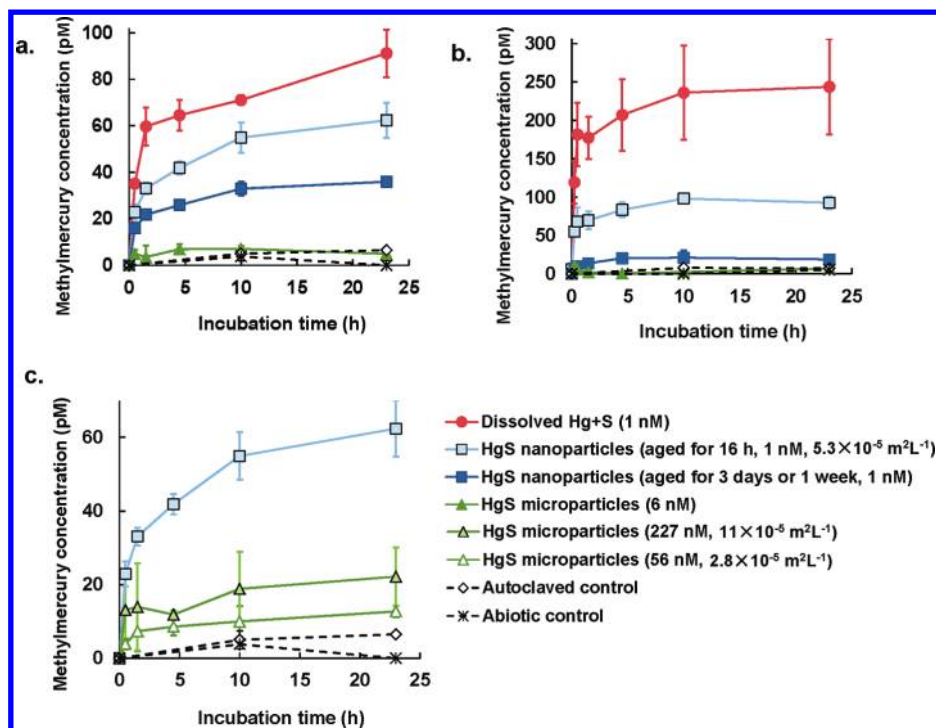


**Figure 1.** Net MeHg production in SRB cultures exposed to different forms of mercuric sulfides. Methylation by (a) *D. propionicus* 1pr3 and (b) *D. desulfuricans* ND132 cultures that were exposed to 1 nM dissolved  $\text{Hg}(\text{NO}_3)_2$  and  $\text{Na}_2\text{S}$ , 1 nM humic-HgS nanoparticles, and 6 nM HgS microparticles. The HgS nanoparticle stock solution was stored at room temperature for 16 h and a longer period (3 days in Figure 1a and 1 week in Figure 1b) prior to amending to cultures. (c) Methylation by *D. propionicus* 1pr3 cultures that were exposed to the similar geometric surface area of HgS nano- and microparticles: 1 nM ( $5 \times 10^{-5} \text{ m}^2 \text{ L}^{-1}$ ) HgS nanoparticles aged for 16 h, 56 nM HgS microparticles ( $3 \times 10^{-5} \text{ m}^2 \text{ L}^{-1}$ ), and 227 nM HgS microparticles ( $11 \times 10^{-5} \text{ m}^2 \text{ L}^{-1}$ ). Autoclaved cultures or abiotic culture media were amended with 1 nM dissolved  $\text{Hg}(\text{NO}_3)_2$  and  $\text{Na}_2\text{S}$ . All cultures received the same humic acid concentration ( $0.2 \mu\text{g-C L}^{-1}$ ). The error bars represent  $\pm 1$  SD of duplicate samples for the controls and triplicate samples in all other experiments.

resin, while the hydrophilic fraction was defined as mercury passing through the  $\text{C}_{18}$ -filter. The concentration of chemically “labile” Hg was quantified from the difference of hydrophilic Hg concentrations in the thiol-amended sample and in the control (i.e., no thiol added).

## RESULTS AND DISCUSSION

**Methylation of Mercury Sulfides.** The net production of MeHg in the cultures varied depending on the type of HgS added (Figure 1). For each SRB strain, the cultures exposed to dissolved  $\text{Hg}(\text{NO}_3)_2$  and  $\text{Na}_2\text{S}$  (and likely to be precipitating HgS in situ) demonstrated the highest net MeHg production. MeHg production was observed to a lesser extent in the nanoparticle exposures. In cultures exposed to HgS microparticles, MeHg concentration was less than 8 pM and similar to the autoclaved and abiotic controls. Furthermore, MeHg production by cultures exposed to nanoparticles depended on the age of the nano-HgS stock solutions. The cultures methylated 6–10% of the total mercury derived from nanoparticles aged for 16 h, whereas cultures methylated a smaller fraction (2–4%) if exposed to older nanoparticles (aged 3 days or 1 week) (Figure 1a and b). Consistent results were obtained in replicate experiments employing higher mercury doses (5 nM) and longer incubation time (up to 10 days) (SI Figure S1).

Overall, the results demonstrated that the methylation potential of mercury introduced as HgS nanoparticles was greater than bulk scale HgS particles. These results were not due to differences in cell growth, as the optical density ( $\text{OD}_{660}$ )

and protein content were identical in all HgS exposures (SI Figure S2). In the *D. propionicus* 1pr3 cultures,  $\text{OD}_{660}$  increased from 0.27 to 0.31 (or a specific growth rate  $\mu$  of  $0.0050 \text{ h}^{-1}$ ) and total protein concentration increased from 9.5 to  $14.1 \mu\text{g/mL}$  ( $\mu = 0.017 \text{ h}^{-1}$ ) after one day of incubation. In the *D. desulfuricans* ND132 cultures,  $\text{OD}_{660}$  increased from 0.23 to 0.35 ( $\mu = 0.017 \text{ h}^{-1}$ ) and total protein concentration increased from 26.1 to  $49.5 \mu\text{g/mL}$  ( $\mu = 0.027 \text{ h}^{-1}$ ) after one day of incubation.

The differences of methylation between the nanoparticle and microparticle exposures were likely due to geochemical Hg speciation rather than growth rates of the cultures. The diameter of the nanoparticles was smaller (3–4 nm) and specific surface area was larger ( $220\text{--}260 \text{ m}^2 \text{ g}^{-1}$ ) compared to the microparticles ( $>500 \text{ nm}$ ,  $2.5 \text{ m}^2 \text{ g}^{-1}$ ) (Table 1, SI Figure S3 and S4). While the surface composition of Hg and S was similar for the nano- and micro-HgS, as shown by X-ray photoelectron spectroscopy (SI Figure S5a and S5b), the degree of crystallinity varied between nano- and microparticles. X-ray diffraction and electron diffraction data suggested that the nanoparticles were poorly crystalline compared to the HgS microparticles (SI Figure S4 and S5c).

While nanoparticles generally have high specific surface areas relative to their bulk scale analogs, they can also exhibit unique reactivity due to lattice or surface imperfections that occur with nanoscale particles.<sup>18,31</sup> Here, we provide two lines of evidence to demonstrate that biomethylation of HgS nanoparticles did not depend simply on surface area. First, as the HgS nanoparticles were allowed to age for 16 h and 3 days prior

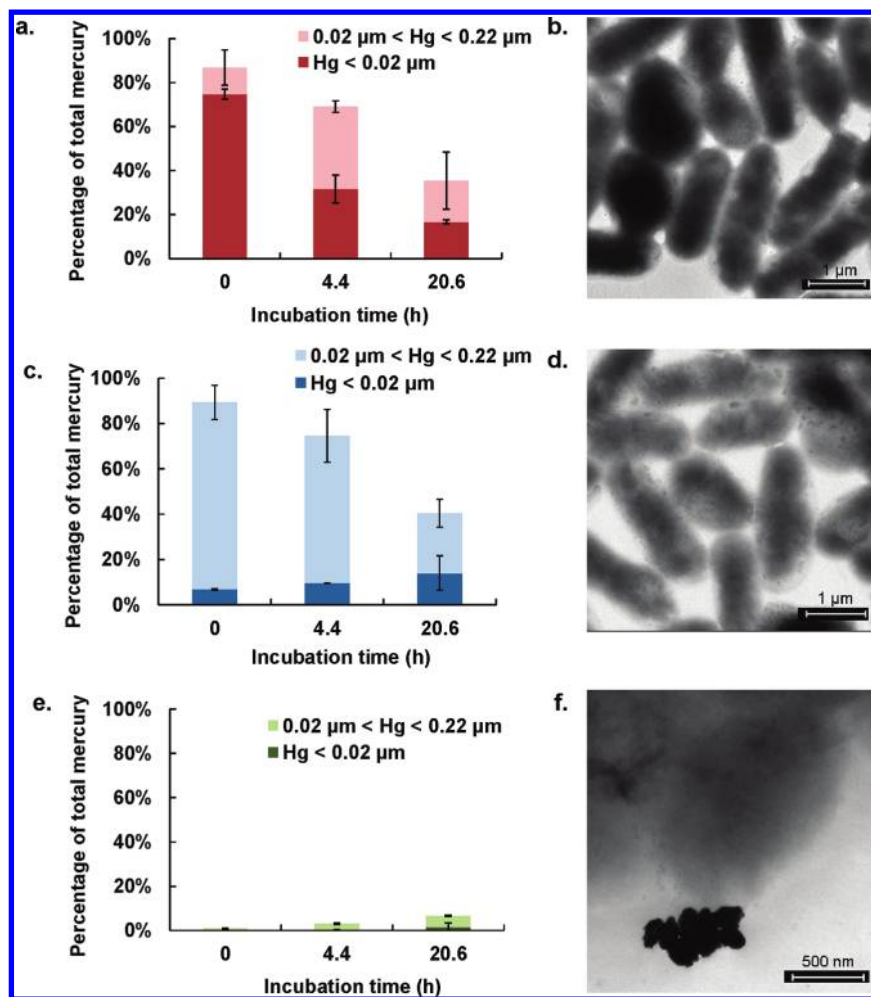


**Figure 2.** Percentages of mercury in solution after filtration of *D. propionicus* 1pr3 cultures and TEM images of the cultures. Cultures were exposed to 1 nM dissolved  $\text{Hg}(\text{NO}_3)_2$  and  $\text{Na}_2\text{S}$  (a and b); 1 nM humic-HgS nanoparticles (aged for 16 h, c and d); and 6 nM HgS microparticles (e and f). “Hg < 0.02  $\mu\text{m}$ ” represents the fraction of total mercury that passed through 0.02  $\mu\text{m}$  filters. “0.02  $\mu\text{m}$  < Hg < 0.22  $\mu\text{m}$ ” represents the concentration difference of aliquots filtered by 0.22  $\mu\text{m}$  or 0.02  $\mu\text{m}$  filters. Cells for TEM image were collected 14 h after exposure to HgS. The error bars represent  $\pm 1$  SD for duplicate samples.

to exposure to *D. propionicus* 1pr3, their methylation potential was considerably reduced (Figure 1a) while their size and specific surface area remained similar (Table 1). Statistically significant differences in geometric surface area and monomer diameter were observed only with the 1-week old nanoparticles.

Second, nano-HgS was more reactive per unit surface area relative to micro-HgS. MeHg generated from nano-HgS with  $5.3 \times 10^{-5} \text{ m}^2 \text{ L}^{-1}$  surface area was 3 times greater than MeHg generated from micro-HgS with  $11 \times 10^{-5} \text{ m}^2 \text{ L}^{-1}$  surface area (Figure 1c), corresponding to a production of MeHg per  $\text{m}^2$  of material that was 6 times higher for nano-HgS compared to micro-HgS (1.13  $\mu\text{mol m}^{-2}$  and 0.18  $\mu\text{mol m}^{-2}$ , respectively). The reduced availability of nano-HgS during aging may be due to the structural changes occurring with amorphous nanoparticles or cluster/particles at the small size range (1–2 nm). These changes would not be reflected in the diameter and specific surface area measurements from TEM or XRD analyses. Due to sample preparation and analysis requirements, these methods are not quantitative reflections of all forms of mercury in the nano-HgS stock solution, and the data are likely to be biased toward more crystalline particles.

The net production of methylmercury was relatively fast in the first few hours and slow after this initial time period (Figure

1). This deceleration of MeHg production could not be explained by microbial growth, as we observed a steady increase of cell density throughout the one-day mercury methylation experiments (SI Figure S2). Similar trends were observed in other mercury methylation studies using the same SRB strains<sup>5,23</sup> and estuarine sediment slurries.<sup>32</sup> These results are possibly due to the saturation of enzymes and/or depletion of certain compounds (e.g., methyl donors) that are required for mercury methylation. Furthermore, inorganic Hg speciation may have shifted after the first few hours toward less bioavailable forms for the bacteria. The declining net methylation rate may also be explained by the contribution of a reverse process (i.e., methylmercury degradation) balancing overall methylmercury concentrations in the cultures. *Desulfovibrio desulfuricans* ND132 and *Desulfobulbus propionicus* strains are known to simultaneously generate and degrade MeHg.<sup>23,33,34</sup> We performed experiments with the 1pr3 strain exposed to methylmercury chloride and observed MeHg degradation in these cultures (SI Figure S6).

**Mercury Fractionation in Methylating Cultures.** In cultures exposed to the three forms of mercury, we fractionated the mercury into nominally dissolved mercury (<0.02  $\mu\text{m}$ ), colloidal mercury (between 0.02 and 0.22  $\mu\text{m}$ ), and particulate

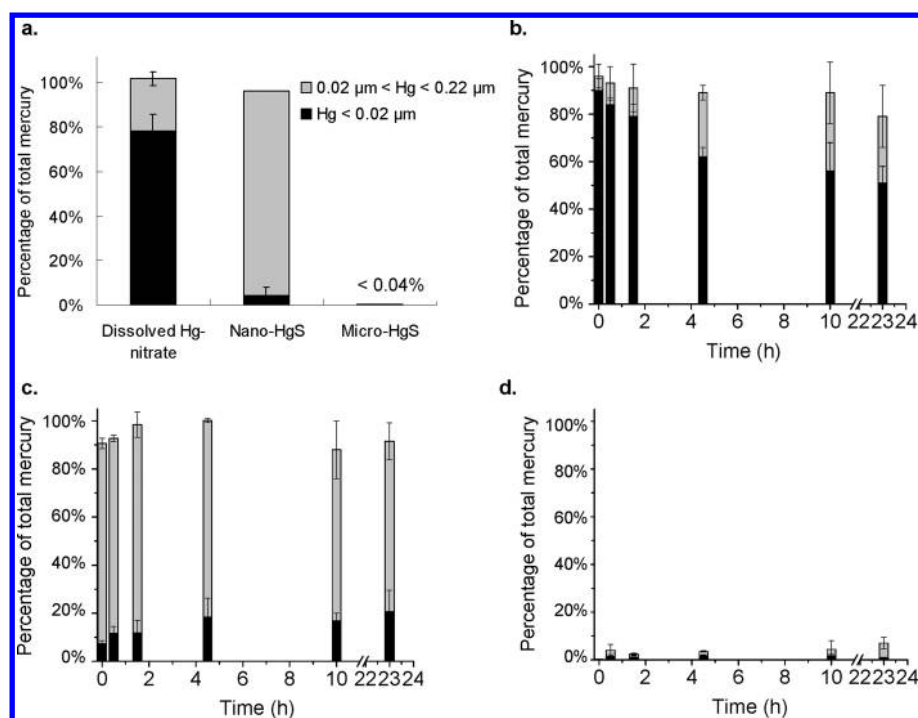


**Figure 3.** Filtration of mercury-amended bacteria-free media (for culturing *D. propionicus* 1pr3). (a) Medium solution was amended with 1 nM  $\text{Hg}(\text{NO}_3)_2$ , 1 nM humic-HgS nanoparticles (aged for 16 h) or 6 nM HgS microparticles, and filtered immediately (less than 10 min) after mercury addition. Filtration of separate samples at different time points after they were amended with different Hg-sulfide species, including (b) 1 nM dissolved  $\text{Hg}(\text{NO}_3)_2$  and  $\text{Na}_2\text{S}$ , (c) 1 nM humic-HgS nanoparticles (aged for 16 h), and (d) 6 nM HgS microparticles. “ $\text{Hg} < 0.02 \mu\text{m}$ ” represents the fraction of total mercury that passed through  $0.02\text{-}\mu\text{m}$  filters. “ $0.02 \mu\text{m} < \text{Hg} < 0.22 \mu\text{m}$ ” represents the concentration difference of aliquots filtered by  $0.22 \mu\text{m}$  or  $0.02 \mu\text{m}$  filters. The error bars represent  $\pm 1$  SD for duplicate samples.

or cell-associated mercury ( $>0.22 \mu\text{m}$ ) using filters with two different pore sizes ( $0.02$  and  $0.22 \mu\text{m}$ ) (Figure 2). Bacteria-free media that were amended with dissolved  $\text{HgNO}_3$ , nanoparticulate HgS, and microparticulate HgS was also filtered in the same manner (Figure 3). The results indicated that the two filters could be used to distinguish these forms of mercury (Figure 3a). We also examined the cultures with transmission electron microscopy (TEM) to further differentiate mercury associated with cells from mercury associated with large aggregates of HgS particles. In the nano-HgS exposures, the filtration results showed that the amount of mercury in the  $>0.22 \mu\text{m}$  fraction increased over incubation time (Figure 2c). In TEM images, on the other hand, large aggregates of HgS particles ( $>0.22 \mu\text{m}$ ), as seen in the micro-HgS treated cultures (Figure 2f and SI Figure S7c), were not observed in the nanoparticle exposures (Figure 2d and SI Figure S7b).

While mercury was quantified in the  $>0.22 \mu\text{m}$  fraction, the nanoparticles were likely too dilute to be observed in bacterial cultures that contained a complex mixture of particles (SI Figure S7b). The nanoparticles could also be dissolving into solution, as indicated by a small increase of dissolved mercury (from  $0.073$  nM to  $0.21$  nM in one day) in bacteria-free media amended with 1 nM nano-HgS (Figure 3c). This concentration range is greater than would be expected from the equilibrium solubility of  $\beta\text{-HgS}_{(s)}$  ( $K_{sp} = 10^{-38.7 \pm 2}$  for the reaction:  $\text{Hg}^{2+} + \text{HS}^- = \text{HgS}_{(s)} + \text{H}^+$ ).<sup>35</sup> Using Hg-sulfide equilibrium equations described in our previous paper,<sup>8</sup> we calculated that in our samples with 1 nM  $\text{Hg}(\text{II})$  and 1 nM  $\text{S}(\text{-II})$  at pH 7.5, dissolved Hg concentration at equilibrium with  $\text{HgS}_{(s)}$  should be  $10^{-9}$  to  $10^{-5}$  nM, depending on the solubility product for  $\text{HgS}_{(s)}$ . In media containing both bacteria and nanoparticles, the percent of total mercury in the  $>0.22 \mu\text{m}$  fraction was 60% after 1 day

and greater than bacteria-free media containing nanoparticles (8%) (Figure 2c and Figure 3c), indicating that the nanoparticles were either depositing onto cells or releasing dissolved mercury that was immediately adsorbed to or taken up by the cells. Micro-HgS was less accessible for biomethylation, possibly due to the minimal or slow mercury dissolution ( $<0.02$  nM mercury dissolved in the bacteria free experiments, Figure 3d).

In the dissolved Hg+S and nano-HgS exposures, the amount of mercury in the  $>0.22 \mu\text{m}$  fraction was similar (Figure 2a and c), yet these treatments exhibited markedly different MeHg production (SI Figure S8). While HgS clusters and nanoparticles were likely forming in the cultures receiving dissolved  $\text{Hg}(\text{II})$  and  $\text{S}(\text{-II})$ , net MeHg production was faster in the dissolved mercury exposure than the nanoparticle exposure. These results agree with recent studies that suggested transmembrane mercury uptake as the rate-limiting step of intracellular mercury methylation<sup>34,36</sup> and imply that HgS nanoparticles are not as bioavailable as their precursors (e.g., dissolved mercury-sulfide complexes and clusters). Similar patterns of mercury size fractionation were observed in replicate cultures processed by centrifugation and ultracentrifugation (SI Figure S9).

#### Mercury Speciation by Competitive Ligand Exchange.

We applied competitive ligand exchange-solid phase extraction<sup>29,30</sup> to further examine the ligand exchange reactivity of mercury in bacteria-free media. In this method, labile mercury species were replaced by Hg–thiol complexes: either hydrophilic mercury–glutathione (GSH) complexes or hydrophobic Hg–diethyldithiocarbamate (DEDIC) complexes. Labile mercury was quantified by the change of mercury in the hydrophilic fraction (defined as mercury passing through a  $\text{C}_{18}$ -resin filter).

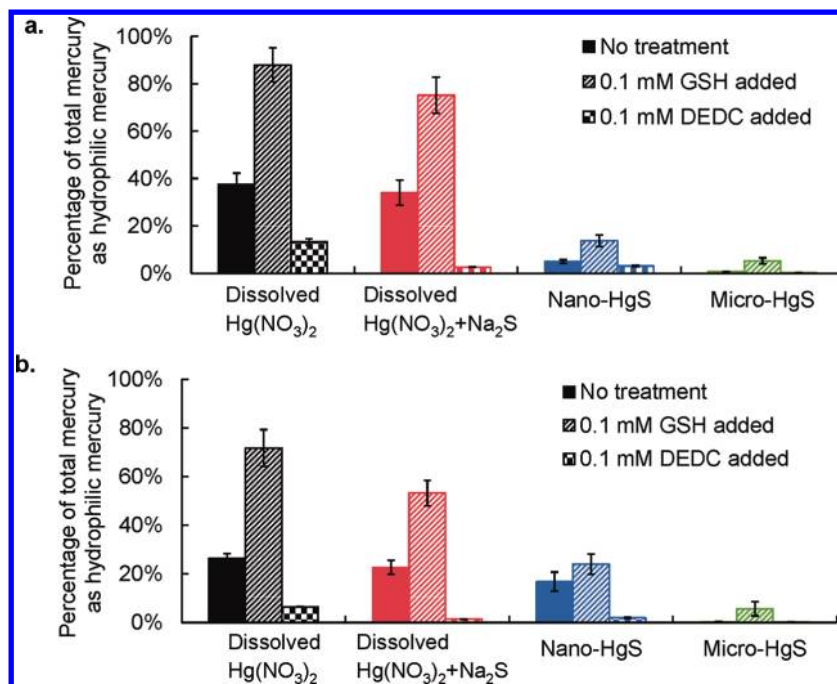


**Figure 4.** Hydrophilic mercury in HgS-amended media after competitive ligand exchange with GSH or DEDC and  $C_{18}$  solid-phase extraction. Uninoculated medium solutions (for culturing *D. propionicus* 1pr3) were spiked with 1 nM dissolved  $Hg(NO_3)_2$ , 1 nM dissolved  $Hg(NO_3)_2$  and  $Na_2S$ , 1 nM humic-HgS nanoparticles (aged for 16 h), and 6 nM HgS microparticles. Ligand exchange reactions were performed by amending aliquots of these samples with GSH or DEDC at two time points after the mercury amendment: (a) Immediately (less than 10 min). (b) 23 h. GSH and DEDC were mixed in the samples for 1 h and then filtered through a  $C_{18}$  resin. All solutions received the same humic acid concentration (0.2  $\mu\text{g-C/L}$ ). Error bars represent  $\pm 1$  SD for duplicate samples.

In the micro-HgS exposure, mercury speciation remained unchanged after addition of GSH or DEDC (Figure 4), indicating that mercury was largely inert. In the media containing nano-HgS, the amount of hydrophilic mercury increased after 1 day, and this fraction was mostly removed by DEDC ligand exchange (Figure 4b), indicating the presence of labile mercury. However, in the dissolved Hg+S exposure, the changes in the hydrophilic mercury fraction after addition of GSH and DEDC were both larger than in the nano-HgS treatment. This pattern of decreasing thiol-exchange reactivity between the dissolved, nanoparticulate and microparticulate mercury corresponded to decreasing methylation rates (Figure 1). Mercury is believed to bind to bacterial cells through thiol-containing ligands on the membrane surfaces,<sup>37</sup> and these complexes may enter the cells as favorable substrates for methylation.<sup>36</sup> Hence, the labile mercury quantified by thiol ligand exchange could signify the available fraction of mercury for microbial uptake and methylation.

**Environmental Implications.** Our overall results have shown that mercury bioavailability (and methylation potential) is not adequately represented by equilibrium speciation of aqueous dissolved mercury (defined by a 0.2 or 0.4  $\mu\text{m}$  filter).<sup>6</sup> Our previous work<sup>8</sup> has suggested that  $HgS^0_{(aq)}$  (a form of dissolved mercury presumed to be bioavailable<sup>6</sup>) may represent HgS nanoparticles rather than a mononuclear aqueous mercury-sulfide complex.

Bacteria are not known to directly take up nanoparticles without compromising their membrane integrity. Moreover, previous works have indicated that bacteria can take up metal constituents of nanoparticles through the dissolution of nanoparticles that accumulated at cell surfaces.<sup>19–21</sup> Indeed, a mechanism of direct uptake of nanoparticles is not necessary for explaining the data presented here. Instead, our results

suggest that bioavailability is related to the kinetics of reactions (rates of cluster formation, crystal ripening, dissolution, etc.).

Therefore, a single entity to represent nanoparticulate or colloidal HgS is overly simplistic. The bioavailability of mercury depends on the evolving nanoscale properties of mercury compounds that fall in the fraction typically designated as dissolved and colloidal (less than 0.2 or 0.45  $\mu\text{m}$ ). This conclusion could help explain observations that mercury recently deposited to surface waters from the atmosphere (as weak  $HgCl_2$  complexes) is more readily transformed to MeHg than older mercury that persists mainly as crystalline  $HgS_{(s)}$  in historically contaminated sediments.<sup>38,39</sup>

Although the occurrence of nanoparticulate or colloidal HgS has been suggested in a number of studies,<sup>8–11,30,40,41</sup> our investigation is the first to explore the potential of HgS nanoparticles to serve as an important, but previously unrecognized source of bioavailable mercury for methylating bacteria. Overall, our results point to a new approach that should consider reaction mechanisms and Hg transformation kinetics for modeling mercury bioavailability. Such models could facilitate prediction and mitigation of MeHg hotspots in the aquatic environment. Given that mineral nanoparticles are ubiquitous in the environment,<sup>18</sup> the importance of nanoscale processes for trace metal bioavailability and toxicity has yet to be fully realized. Our findings provide a new approach that may be applied to other metal-sulfide nanoparticles (e.g., ZnS, CuS, FeS) and their potential roles in biogeochemical metal cycling.

## ■ ASSOCIATED CONTENT

### 📄 Supporting Information

Additional methodology details regarding the characterization of the HgS particles, methylmercury biodegradation experiments, and centrifugation experiments. SI figures include

replication of the mercury biomethylation experiments, optical density and protein content of the cultures, characterization of the HgS particles (DLS, TEM, XPS, and XRD), degradation of MeHg by 1pr3, and fractionation of mercury in the cultures by centrifugation. This material is available free of charge via the Internet at <http://pubs.acs.org>.

## AUTHOR INFORMATION

### Corresponding Author

\*Phone: (919) 660-5109; fax: (919) 660-5219; e-mail: [hsukim@duke.edu](mailto:hsukim@duke.edu);

## ACKNOWLEDGMENTS

We thank C. C. Gilmour for the *D. desulfuricans* ND132 culture, K. Ikuma, M. Hochella, G. E. Brown, M. Gignac, and R. Garcia for experimental assistance. This research was supported by the Department of Defense Strategic Environmental Research and Development Program (ER-1744) and the Center for Environmental Implications of NanoTechnology (NSF and EPA, EF-0830093). Portions of this research were carried out at the Stanford Synchrotron Radiation Laboratory, a national user facility operated by Stanford University on behalf of the U.S. Department of Energy, Office of Basic Energy Sciences.

## REFERENCES

- (1) Compeau, G. C.; Bartha, R. Sulfate-reducing bacteria—Principal methylators of mercury in anoxic estuarine sediment. *Appl. Environ. Microbiol.* **1985**, *50* (2), 498–502.
- (2) Ranchou-Peyruse, M.; Monperrus, M.; Bridou, R.; Duran, R.; Amouroux, D.; Salvado, J. C.; Guyoneaud, R. Overview of mercury methylation capacities among anaerobic bacteria including representatives of the sulphate-reducers: implications for environmental studies. *Geomicrobiol. J.* **2009**, *26* (1), 1–8.
- (3) Jensen, S.; Jernelov, A. Biological methylation of mercury in aquatic organisms. *Nature* **1969**, *223* (5207), 753–754.
- (4) Merritt, K. A.; Amirbahman, A. Mercury methylation dynamics in estuarine and coastal marine environments—A critical review. *Earth Sci. Rev.* **2009**, *96* (1–2), 54–66.
- (5) Benoit, J. M.; Gilmour, C. C.; Mason, R. P. Aspects of bioavailability of mercury for methylation in pure cultures of *Desulfobulbus propionicus* (1pr3). *Appl. Environ. Microbiol.* **2001**, *67* (1), 51–58.
- (6) Benoit, J. M.; Gilmour, C. C.; Mason, R. P.; Heyes, A. Sulfide controls on mercury speciation and bioavailability to methylating bacteria in sediment pore waters. *Environ. Sci. Technol.* **1999**, *33* (6), 951–957.
- (7) Drott, A.; Lambertsson, L.; Bjorn, E.; Skjellberg, U. Importance of dissolved neutral mercury sulfides for methyl mercury production in contaminated sediments. *Environ. Sci. Technol.* **2007**, *41* (7), 2270–2276.
- (8) Deonaraine, A.; Hsu-Kim, H. Precipitation of mercuric sulfide nanoparticles in NOM-containing water: implications for the natural environment. *Environ. Sci. Technol.* **2009**, *43* (7), 2368–2373.
- (9) Barnett, M. O.; Harris, L. A.; Turner, R. R.; Stevenson, R. J.; Henson, T. J.; Melton, R. C.; Hoffman, D. P. Formation of mercuric sulfide in soil. *Environ. Sci. Technol.* **1997**, *31* (11), 3037–3043.
- (10) Lowry, G. V.; Shaw, S.; Kim, C. S.; Rytuba, J. J.; Brown, G. E. Macroscopic and microscopic observations of particle-facilitated mercury transport from new idria and sulphur bank mercury mine tailings. *Environ. Sci. Technol.* **2004**, *38* (19), 5101–5111.
- (11) Patty, C.; Barnett, B.; Mooney, B.; Kahn, A.; Levy, S.; Liu, Y. J.; Pianetta, P.; Andrews, J. C. Using X-ray microscopy and Hg L-3 XAMES to study Hg binding in the rhizosphere of *Spartina cordgrass*. *Environ. Sci. Technol.* **2009**, *43* (19), 7397–7402.
- (12) Diaz, X.; Johnson, W. P.; Fernandez, D.; Naftz, D. L. Size and elemental distributions of nano- to micro-particulates in the geochemically-stratified Great Salt Lake. *Appl. Geochem.* **2009**, *24* (9), 1653–1665.
- (13) Guentzel, J. L.; Powell, R. T.; Landing, W. M.; Mason, R. P. Mercury associated with colloidal material in an estuarine and an open-ocean environment. *Mar. Chem.* **1996**, *55* (1–2), 177–188.
- (14) Stordal, M. C.; Gill, G. A.; Wen, L. S.; Santschi, P. H. Mercury phase speciation in the surface waters of three Texas estuaries: importance of colloidal forms. *Limnol. Oceanogr.* **1996**, *41* (1), 52–61.
- (15) Aiken, G. R.; Hsu-Kim, H.; Ryan, J. N. Influence of dissolved organic matter on the environmental fate of metals, nanoparticles, and colloids. *Environ. Sci. Technol.* **2011**, *45* (8), 3196–3201.
- (16) Labrenz, M.; Druschel, G. K.; Thomsen-Ebert, T.; Gilbert, B.; Welch, S. A.; Kemner, K. M.; Logan, G. A.; Summons, R. E.; De Stasio, G.; Bond, P. L.; Lai, B.; Kelly, S. D.; Banfield, J. F. Formation of sphalerite (ZnS) deposits in natural biofilms of sulfate-reducing bacteria. *Science* **2000**, *290* (5497), 1744–1747.
- (17) Moreau, J. W.; Weber, P. K.; Martin, M. C.; Gilbert, B.; Hutcheon, I. D.; Banfield, J. F. Extracellular proteins limit the dispersal of biogenic nanoparticles. *Science* **2007**, *316* (5831), 1600–1603.
- (18) Hochella, M. F.; Lower, S. K.; Maurice, P. A.; Penn, R. L.; Sahai, N.; Sparks, D. L.; Twining, B. S. Nanominerals, mineral nanoparticles, and earth systems. *Science* **2008**, *319* (5870), 1631–1635.
- (19) Bosch, J.; Heister, K.; Hofmann, T.; Meckenstock, R. U. Nanosized iron oxide colloids strongly enhance microbial iron reduction. *Appl. Environ. Microbiol.* **2010**, *76* (1), 184–189.
- (20) Dehner, C. A.; Barton, L.; Maurice, P. A.; Dubois, J. L. Size-dependent bioavailability of hematite ( $\alpha$ -Fe<sub>2</sub>O<sub>3</sub>) nanoparticles to a common aerobic bacterium. *Environ. Sci. Technol.* **2011**, *45* (3), 977–983.
- (21) Glasauer, S.; Langley, S.; Beveridge, T. J. Sorption of Fe (hydr)oxides to the surface of *Shewanella putrefaciens*: cell-bound fine-grained minerals are not always formed de novo. *Appl. Environ. Microbiol.* **2001**, *67* (12), 5544–5550.
- (22) Lowry, O. H.; Rosebrough, N. J.; Farr, A. L.; Randall, R. J. Protein measurement with the folin phenol reagent. *J. Biol. Chem.* **1951**, *193* (1), 265–275.
- (23) Gilmour, C. C.; Elias, D. A.; Kucken, A. M.; Brown, S. D.; Palumbo, A. V.; Schadt, C. W.; Wall, J. D. The sulfate-reducing bacterium *Desulfovibrio desulfuricans* ND132 as a model for understanding bacterial mercury methylation. *Appl. Environ. Microbiol.* **2011**, *77* (12), 3938–3951.
- (24) Institute of Experimental Mineralogy, Russian Academy of Science. *Crystallographic and Crystallochemical Database for Minerals and their Structural Analogues* Created 1997, Updated 2009 (<http://database.iem.ac.ru/mincryst/index.php>).
- (25) Birks, L. S.; Friedman, H. Particle size determination from X-ray line broadening. *J. Appl. Phys.* **1946**, *17* (8), 687–691.
- (26) Kim, C. S.; Bloom, N. S.; Rytuba, J. J.; Brown, G. E. Mercury speciation by X-ray absorption fine structure spectroscopy and sequential chemical extractions: A comparison of speciation methods. *Environ. Sci. Technol.* **2003**, *37* (22), 5102–5108.
- (27) *Method 1630: Methyl Mercury in water by Distillation, Aqueous Ethylation, Purge and Trap, and CVAFS*; U.S., Environmental Protection Agency: Washington, DC, 2001.
- (28) *Method 1631, Revision D: Mercury in Water by Oxidation, Purge and Trap, and Cold Vapor Atomic Fluorescence Spectroscopy*; U.S. Environmental Protection Agency: Washington, DC, 2001.
- (29) Hsu, H.; Sedlak, D. L. Strong Hg(II) complexation in municipal wastewater effluent and surface waters. *Environ. Sci. Technol.* **2003**, *37* (12), 2743–2749.
- (30) Hsu-Kim, H.; Sedlak, D. L. Similarities between inorganic sulfide and the strong Hg(II)—Complexing ligands in municipal wastewater effluent. *Environ. Sci. Technol.* **2005**, *39* (11), 4035–4041.
- (31) Waychunas, G. A.; Zhang, H. Z. Structure, chemistry, and properties of mineral nanoparticles. *Elements* **2008**, *4* (6), 381–387.

- (32) King, J. K.; Saunders, F. M.; Lee, R. F.; Jahnke, R. A. Coupling mercury methylation rates to sulfate reduction rates in marine sediments. *Environ. Toxicol. Chem.* **1999**, *18* (7), 1362–1369.
- (33) Pak, K. R.; Bartha, R. Mercury methylation and demethylation in anoxic lake sediments and by strictly anaerobic bacteria. *Appl. Environ. Microbiol.* **1998**, *64* (3), 1013–1017.
- (34) Bridou, R.; Monperrus, M.; Gonzalez, P. R.; Guyoneaud, R.; Amouroux, D. Simultaneous determination of mercury methylation and demethylation capacities of various sulfate-reducing bacteria using species-specific isotopic tracers. *Environ. Toxicol. Chem.* **2011**, *30* (2), 337–344.
- (35) Smith, R. D.; Martell, A. E. NIST Critical Stability Constants of Metal Complexes Database v. 2.0. 1993.
- (36) Schaefer, J. K.; Morel, F. M. M. High methylation rates of mercury bound to cysteine by *Geobacter sulfurreducens*. *Nat. Geosci.* **2009**, *2* (2), 123–126.
- (37) Mishra, B.; Fein, J.; Yee, N.; Beveridge, T.; Myneni, S. Hg(II) adsorption and speciation on bacterial surfaces. *Geochim. Cosmochim. Acta* **2010**, *74* (12), A713–A713.
- (38) Munthe, J.; Bodaly, R. A.; Branfireun, B. A.; Driscoll, C. T.; Gilmour, C. C.; Harris, R.; Horvat, M.; Lucotte, M.; Malm, O. Recovery of mercury-contaminated fisheries. *Ambio* **2007**, *36* (1), 33–44.
- (39) Harris, R. C.; Rudd, J. W. M.; Amyot, M.; Babiarz, C. L.; Beaty, K. G.; Blanchfield, P. J.; Bodaly, R. A.; Branfireun, B. A.; Gilmour, C. C.; Graydon, J. A.; Heyes, A.; Hintelmann, H.; Hurley, J. P.; Kelly, C. A.; Krabbenhoft, D. P.; Lindberg, S. E.; Mason, R. P.; Paterson, M. J.; Podemski, C. L.; Robinson, A.; Sandilands, K. A.; Southworth, G. R.; Louis, V. L. S.; Tate, M. T. Whole-ecosystem study shows rapid fish-mercury response to changes in mercury deposition. *Proc. Natl. Acad. Sci. U.S.A.* **2007**, *104* (42), 16586–16591.
- (40) Slowey, A. J. Rate of formation and dissolution of mercury sulfide nanoparticles: The dual role of natural organic matter. *Geochim. Cosmochim. Acta* **2010**, *74* (16), 4693–4708.
- (41) Gerbig, C. A.; Kim, C. S.; Stegemeier, J. P.; Ryan, J. N.; Aiken, G. R. Formation of nanocolloidal metacinnabar in mercury-DOM-sulfide systems. *Environ. Sci. Technol.* **2011**, *45* (21), 9180–9187.